

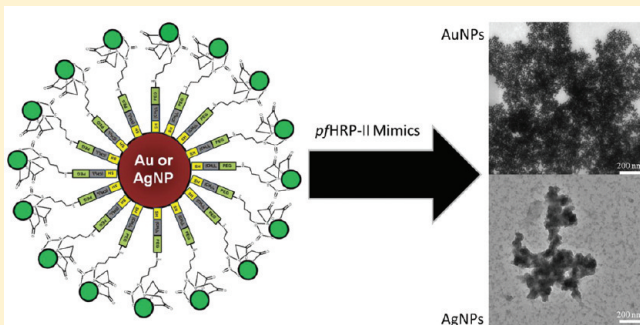
# Development of a Histidine-Targeted Spectrophotometric Sensor Using Ni(II)NTA-Functionalized Au and Ag Nanoparticles

Joshua D. Swartz,<sup>†</sup> Christopher P. Gulka,<sup>†</sup> Frederick R. Haselton,<sup>‡</sup> and David W. Wright<sup>\*,†</sup>

<sup>†</sup>Department of Chemistry and <sup>‡</sup>Department of Biomedical Engineering, Vanderbilt University, Station B 351822, Nashville, Tennessee 37235-1822, United States

## Supporting Information

**ABSTRACT:** An antibody-free diagnostic reagent has been developed based on the aggregation-induced colorimetric change of Ni(II)NTA-functionalized colloidal gold and silver nanoparticles. This diagnostic strategy utilizes the high binding affinity of histidine-rich proteins with Ni(II)NTA to capture and cross-link the histidine-rich protein mimics with the silver and gold nanoparticles. In model studies, the aggregation behavior of the Ni(II)NTA nanoparticles was tested against synthetic targets including charged poly(amino acid)s (histidine, lysine, arginine, and aspartic acid) and mimics of *Plasmodium falciparum* histidine-rich protein 2 (*pf*HRP-II). Aggregation of the nanoparticle sensor was induced by all of the basic poly(amino acid)s including poly(L-histidine) within the pH range (5.5–9.0) tested, which is likely caused by the coordination between the multivalent polymer target and Ni(II)NTA groups on multiple particles. The peptide mimics induced aggregation of the nanoparticles only near their  $pK_a$ 's with higher limits of detection. In addition, monomeric amino acids do not show any aggregation behavior, suggesting that multiple target binding sites are necessary for aggregation. Long-term stability studies showed that gold but not silver nanoparticles remained stable and exhibited similar aggregation behavior after 1 month of storage at room temperature and 37 °C. These results suggest that Ni(II)NTA gold nanoparticles could be further investigated for use as a sensor to detect histidine-rich proteins in biological samples.



## INTRODUCTION

Throughout the developing world, the cost of diagnosis is a significant barrier to effective distribution of limited public health resources. It is often difficult to reach sparsely populated regions with either standard or sophisticated diagnostic equipment due to the difficult terrain, intermittent availability of electricity and clean water, and lack of a skilled workforce. To circumvent these challenges, rapid diagnostic tests (RDTs) have been developed for infectious diseases such as malaria that provide a self-contained immunochromatographic test delivering infectivity results within 15–30 min.<sup>1</sup> Although RDTs perform well in a laboratory setting, their reliance on the antibody–biomarker interaction renders them thermally sensitive in subtropical regions of the world. Recent performance testing conducted by the World Health Organization (WHO) found that most commercially available antibody-based malaria RDTs when exposed to higher storage temperatures performed poorly at the recommended lower limit of detection of 200 parasites/ $\mu\text{L}$ .<sup>2</sup> Therefore, rapid diagnostics based on thermally stable reagents would improve their utility in applications where refrigeration is not available.

Because of their unique physical and chemical properties, gold and silver nanoparticles (AuNPs and AgNPs, respectively) have been used as diagnostic sensors.<sup>3–8</sup> Both of these nanoparticles exhibit a visible surface plasmon resonance induced by the

collective oscillation of electrons at their surfaces, giving them their representative red and yellow colors in aqueous solutions. Since the nanoparticles have a high surface area to volume ratio, the plasmon frequency is sensitive to the dielectric nature of its interface with the surrounding solution. As interparticle distances between the NPs are reduced to less than the average particle diameter (i.e., during aggregation), their surface plasmon bands couple, resulting in visible red shifts in absorption.<sup>9</sup> In addition, only small aggregates containing 2–10 particles per cluster are required to drastically shift the plasmon resonance.<sup>10,11</sup>

Another advantage of gold and silver substrates is their reactivity toward thiolated ligands. This allows for the selective functionalization of surface substrates, which can be tuned to detect specific biological or synthetic targets. Surface substrates also serve to stabilize these nanoparticles in a variety of physiologically relevant conditions.<sup>12</sup> Mirkin et al. have previously designed DNA recognition elements by conjugating complementary thiolated surface ligands (mercaptoalkyloligonucleotides) onto different gold nanoparticles that hybridize upon heating, inducing plasmon coupling of the nanoparticles.<sup>3</sup>

Received: July 28, 2011

Revised: October 22, 2011

Published: October 25, 2011



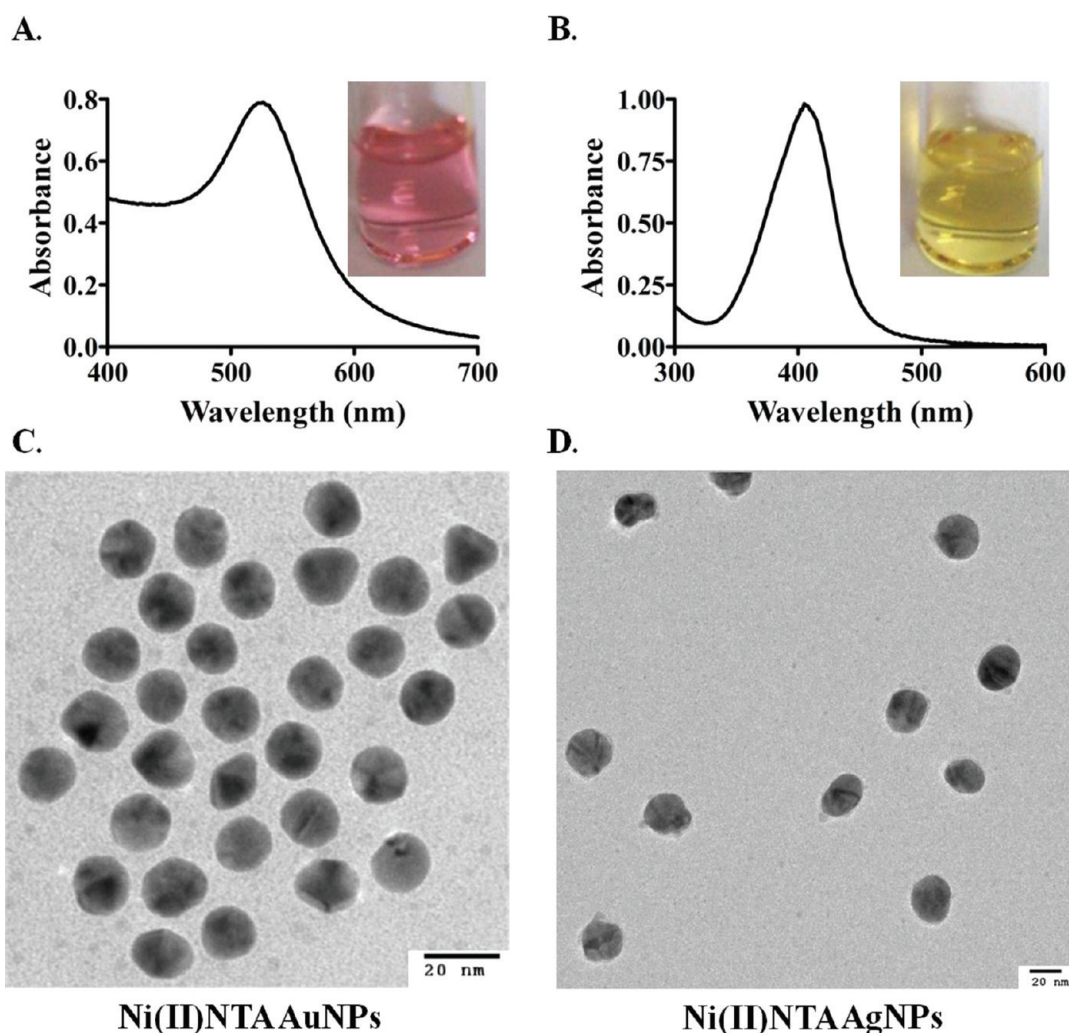


**Figure 1.** Characterization of Ni(II)NTA NPs. UV–vis spectrum of Ni(II)NTA Au (A) and AgNPs (B). TEM images of Ni(II)NTA Au (C) and AgNPs (D).

**Table 1.** Physical Properties of Ni(II)NTA NPs

metal	plasmon absorption peak position (nm)			particle hydrodynamic diameter (nm)		
	citrate NPs	Ni(II)NTA	shift	citrate NPs	Ni(II)NTA	shift
Au	520	525	5	$19.64 \pm 0.25$	$24.24 \pm 0.75$	4.60
Ag	406	411	5	$29.64 \pm 1.33$	$35.67 \pm 0.38$	6.03

the presence of common human serum proteins at physiological concentrations was investigated.

## RESULTS

Ni(II)NTA-functionalized Au and Ag nanoparticles were synthesized following modified procedures developed by Barton et al.<sup>27</sup> The NTA-thiol ligand (**7**) was synthesized (Scheme 1) following modifications of Schmitt et al.<sup>28</sup> and Tinazli et al.<sup>29</sup> Surface functionalization of the Ag and Au nanoparticles was performed by incubating particles overnight with purified NTA-thiol ligand in water, allowing for efficient packing of the ligand onto the surface of the particles (Scheme 2). After incubation, the

NPs were centrifuged and washed three times with buffer (0.1 M HEPES buffer, pH 7.4) to remove any unreacted thiols. The NPs were charged overnight with a solution of NiCl<sub>2</sub>. After purification, the particles were characterized by UV–vis spectroscopy and DLS and imaged with TEM (Figure 1 and Table 1). Both particles show a minimal red shift (~5 nm) in their surface plasmon absorption, which is consistent with the dielectric changes induced by the monolayer of Ni(II)NTA on their surfaces.<sup>27,30</sup> The Ni(II)NTA AuNPs have an average hydrodynamic diameter of  $24.34 \pm 0.74$  nm and the Ni(II)NTA AgNPs are  $35.67 \pm 0.38$  nm, which is 4.6 and 6.03 nm larger than the unfunctionalized stock particles. This particle size increase is consistent with the addition of 7 to their respective surfaces. TEM analysis revealed that the particles are monodisperse, suggesting that they do not aggregate during preparation.

The aggregation behavior of the Ni(II)NTA NPs was examined in the presence of commercially available acidic and basic poly(amino acid)s. At pH 7.4, the poly(amino acid)s poly(L-histidine) (PLH), poly(L-arginine) (PLR), and poly(L-lysine) (PLL), known to have affinity toward Ni(II)NTA, induced aggregation of both the Au and AgNPs. Poly(aspartic acid) (PLD) did not induce aggregation (see Supporting Information

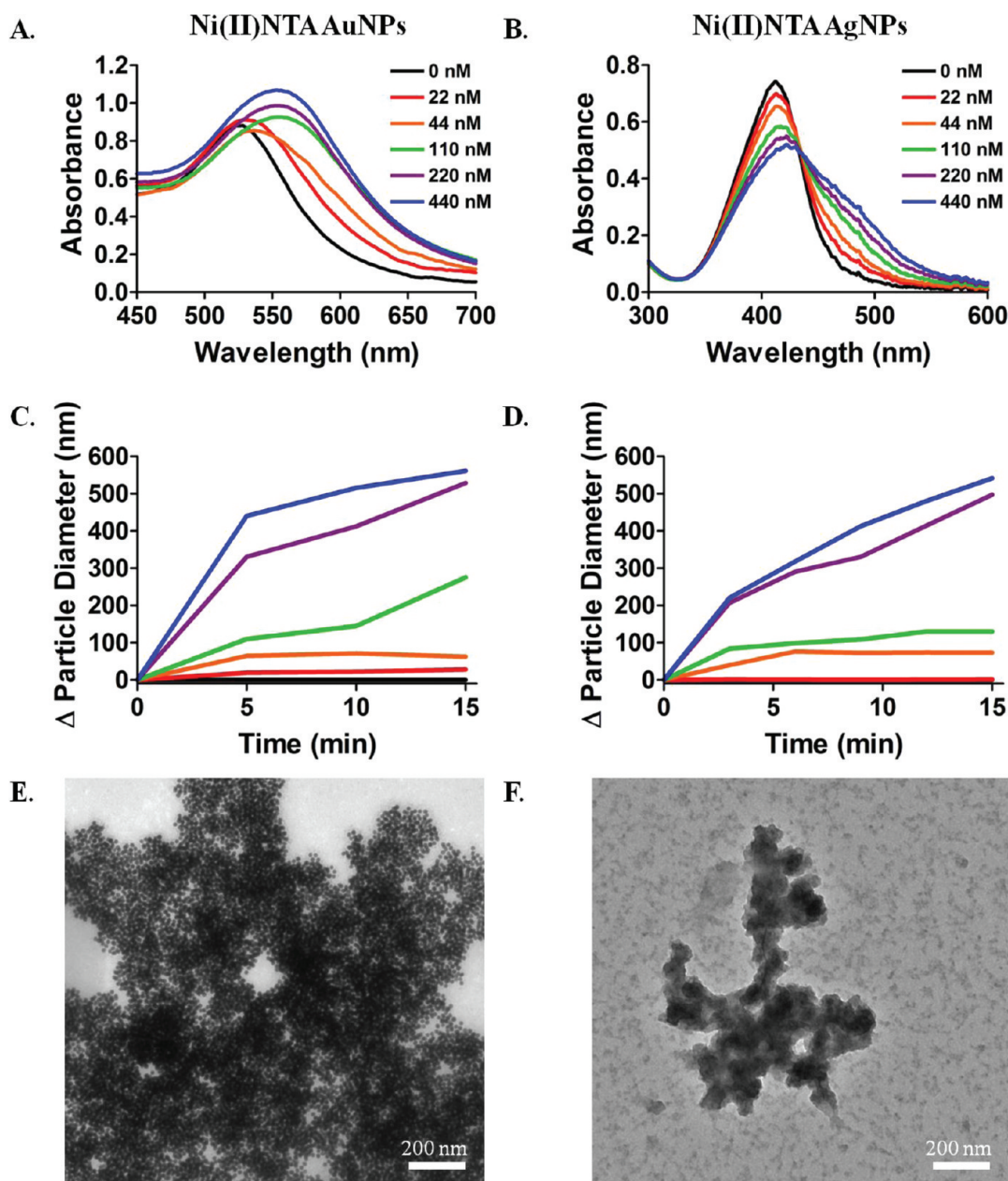


**Figure 2.** Aggregation of Ni(II)NTA AuNPs (left) and AgNPs (right) induced by poly(L-histidine) (PLH). UV-vis of Ni(II)NTA Au (A) and AgNPs (B) in the presence of 0–440 nM PLH. DLS particle hydrodynamic diameter profiles of Ni(II)NTA Au (C) and AgNPs (D). Representative TEM images of Ni(II)NTA AuNPs (E) and AgNPs (F) in the presence of 110 nM PLH. Note that further aggregation has occurred during the preparation of the samples onto the TEM grid.

for PLR, PLL, and PLD titrations). Highlighted in Figure 2 are UV-vis spectra, DLS profiles, and representative TEM images for Ni(II)NTA NPs reacted with PLH over a concentration range of 0–440 nM. UV-vis spectroscopy indicates a red shift caused by PLH-induced cross-linking of the nanoparticles. Significant peak broadening is observed for all concentrations, and the absorption maximum shifts by  $\sim 30$  nm to 555 nm for the highest concentrations for Ni(II)NTA AuNPs. The spectral profile for Ni(II)NTA AgNPs in the presence of PLH indicates a peak broadening shift of  $\sim 70$  to  $\sim 480$  nm. DLS measurements indicated that the average hydrodynamic diameter of both the gold and silver nanoparticle aggregates approached 500 nm as a function of time and target concentration. TEM images further

confirm that the particles form large aggregates as a result of Ni(II)NTA-PLH cross-linking.

Poly(amino acid)-induced aggregation of Ni(II)NTA NP also demonstrated a pH dependence over a range of pH 4 to pH 9. Aggregation of the nanoparticles was detected spectrophotometrically for PLH, PLL, and PLR at all pH's for AgNPs and below 9.0 for AuNPs. Again, PLD showed no aggregation, regardless of the pH (Supporting Information). Figure 3a demonstrates the aggregation behavior of the Ni(II)NTA NPs in the presence of PLH (200 nM) at variable pH (4–10). The % aggregation reported is calculated by taking the ratio of two selected wavelengths ( $A_{600}/A_{525}$  for Au and  $A_{520}/A_{411}$  for Ag) and normalizing the highest ratio value to 100. Titrations with PLH

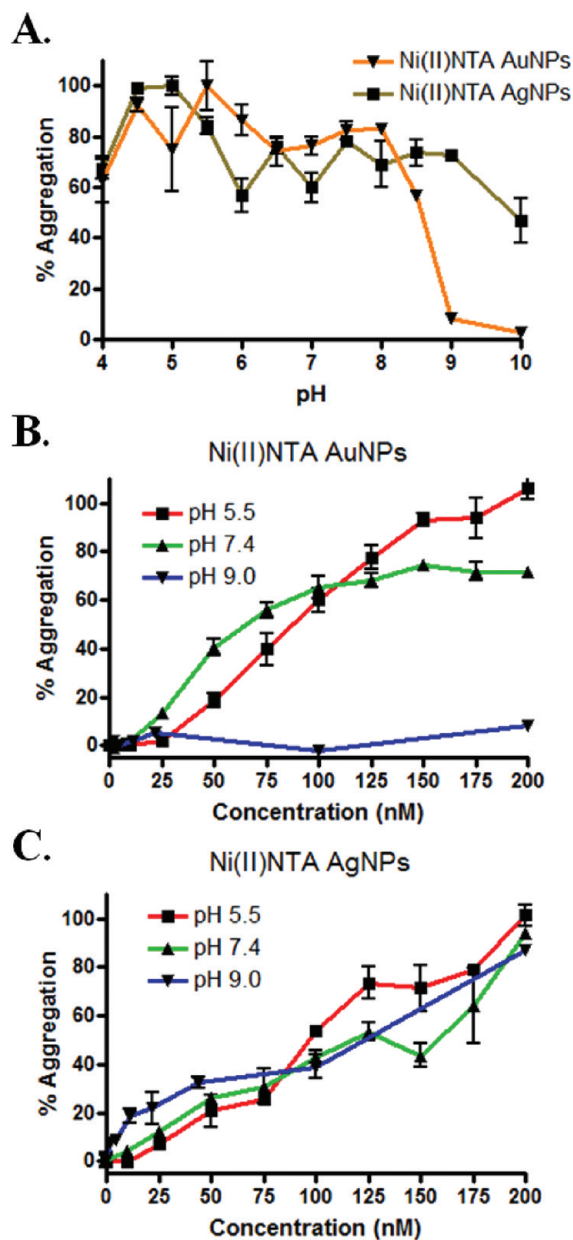


**Figure 3.** Aggregation response of Ni(II)NTA NPs for poly (L-histidine) at variable pH. (A) Aggregation of the particles in the presence of 200 nM PLH at variable pH. (B) Aggregation of Ni(II)NTA AuNPs induced by PLH at variable concentrations of PLH at selected pH's. (C) Aggregation of Ni(II)NTA AgNPs induced by PLH at variable concentrations of PLH at selected pH's. The % aggregation values reported are calculated by normalizing the highest ratio of  $A_{600}/A_{525}$  for Au and  $A_{520}/A_{411}$  for Ag and normalizing to 100.

were also conducted at selected pH's (5.5, 7.4, and 9.0) to determine the limit of detection of aggregation (Figure 3B,C). The limit of detection for aggregation at pH 5.5 was 32.6 nM for Ni(II)NTA AuNPs and 27.4 nM for Ni(II)NTA AgNPs (Table 2).

To understand how the gold and silver sensors interact with a biologically relevant sample, the particles were tested for aggregation behavior in the presence of two peptide mimics of the malarial protein *pf*HRP-II. pHRP-II is a 27 amino acid linear peptide containing the antigenic repeat (AHHAHHAAD)<sub>3</sub>,

**Table 2.** Limits of Detection for the Histidine-Rich Targets Investigated in This Study

	Ni(II)NTA AuNPs		Ni(II)NTA AgNPs	
	limit of detection (nM)	95% confidence intervals (nM)	limit of detection (nM)	95% confidence intervals (nM)
PLH	33	25–39	27	17–36
pHRP-II	620	570–660	490	360–610
BNT-II	190	160–213	100	37–160

targeted by many RDT's. BNT-II is a functional dendrimeric mimic of *pf*HRP-II previously synthesized by Ziegler and co-workers.<sup>31</sup> This peptide contains 4 branched repeats of (AHHAHHAAD)<sub>2</sub>, which provides 16 heme binding motifs (a proposed natural substrate) and a more realistic  $3_{10}$ -helical structure as seen for *pf*HRP-II in the presence of heme.<sup>26</sup> Much like PLH, both mimics induced aggregation of the nanoparticles at pH's below 6.5; however, no particle aggregation was observed at neutral pH or higher (Figure 4). Titrations of the mimic targets at pH 5.5 revealed that the limit of detection of pHRP-II is 620 and 490 nM for Au and AgNPs, respectively. With the more realistic biological mimic BNT-II, the limit of detection is improved to 190 nM for Ni(II)NTA AuNPs and 100 nM for Ni(II)NTA AgNPs (Table 2).

In complex biological mixtures such as human blood or saliva, proteins such as transferrin (TF), histidine-rich glycoprotein (HRG), human serum albumin (HSA), and  $\alpha$ -2 macroglobulin ( $\alpha$ 2) are at high concentrations and could act as interferents to the aggregation assay by inducing nonspecific aggregation. Physiological concentrations of these proteins were incubated with the Ni(II)NTA NPs at pH 5.5, and no aggregation was observed. UV–vis difference spectral profiles of Ni(II)NTA NPs in the presence of the protein targets indicated a slight 2 nm shift for Au and 5 nm shift for Ag of the plasmon absorption without any significant peak broadening (Figure 5). This is in stark contrast to particles reacted with the histidine-rich targets, which showed dramatic shifts in their plasmon absorption to longer wavelengths. In addition, the presence of physiological concentrations of HSA during titrations of BNT-II had little if any effect on the aggregation behavior of the particles (Supporting Information) under a variety of reagent and target concentrations, save for at the lowest concentrations of particles.

The long-term stability of the particles was evaluated by storing the particles at room temperature and 37 °C for several weeks before reacting with PLH. After 4 weeks of storage, the Ni(II)NTA AuNPs showed no indication of storage-induced aggregation and similar aggregation behavior in the presence of PLH, suggesting that these particles are stable throughout the study (Figure 6). In contrast, Ni(II)NTA AgNPs lost most of their aggregation behavior after 2 weeks of storage independent of temperature. These results suggest that Ni(II)NTA AuNPs are significantly more stable than Ni(II)NTA AgNPs.

## DISCUSSION

The unique physical and chemical properties of gold and silver nanoparticles make them powerful reagents for possible low-resource point of care diagnostics. Both particles have high molar extinction coefficients of their surface plasmon resonance absorption ( $3.64 \times 10^8 \text{ M}^{-1} \text{ cm}^{-1}$  for Au and  $8.6 \times 10^9 \text{ M}^{-1} \text{ cm}^{-1}$  for Ag), which allows for spectrophotometric detection of these

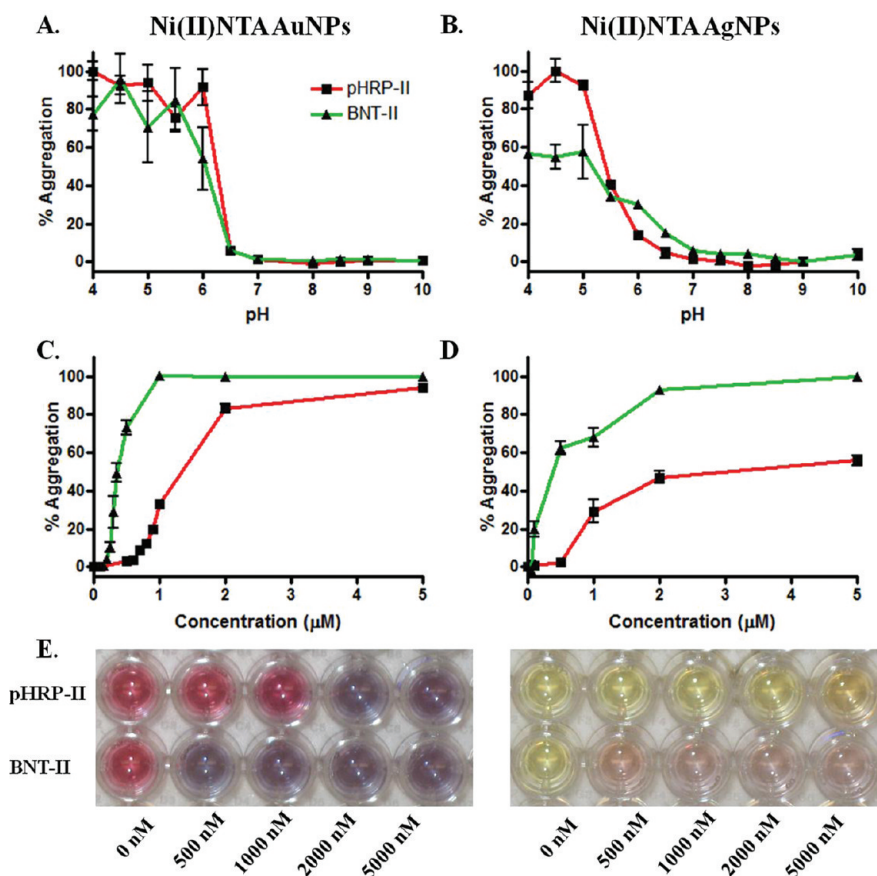


**Figure 4.** Aggregation behavior of Ni(NTA) NPs in the presence of biological mimic targets of the malaria parasite protein *p*fHRP-II. Aggregation of (A) Ni(II)NTA AuNPs and (B) AgNPs in the presence of 2  $\mu\text{M}$  pHRP-II and 500 nM BNT-II at variable pH. Titration of targets with Ni(II)NTA (C) AuNPs and (D) AgNPs at pH 5.5 at variable target concentration. (E) Photographic images of aggregated Ni(II)NTA NPs in the presence of mimics.

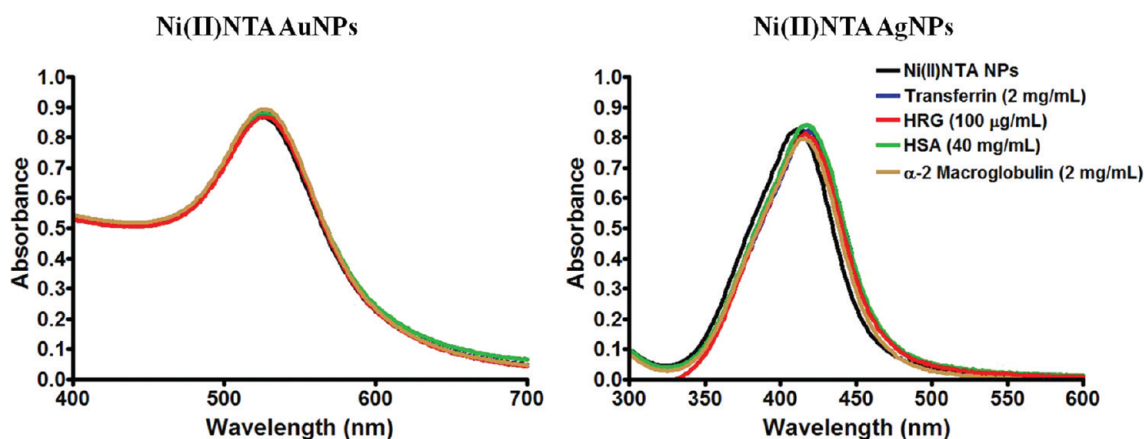


**Figure 5.** UV-vis profiles of Ni(II)NTA (A) AuNPs and (B) AgNPs in the presence of several potential serum protein interferents.

monodisperse particles in the picomolar range. Further, the energy gap of the plasmon band in these particles can increase as aggregation occurs, resulting in a visible red shift in the absorption, which is spectrophotometrically and visibly detectable. This allows for the detection of targets which induce cross-linking of the particles in the nanomolar range of sensitivity.

The key to utilizing such nanoparticles is to endow them with significant selectivity through surface ligand design. The use of a

Ni(II)NTA surface ligand was inspired by nickel affinity chromatography of His-tagged proteins and the realization that *p*fHRP-II is nothing if not a naturally occurring His-tagged protein. For this study, a modular synthetic NTA ligand was designed to include a module for surface functionalization in a well-ordered monolayer, a module to minimize binding of nonspecific interferents, and one to specifically target histidine-rich proteins. The use of a modified alkanethiol ligand provides

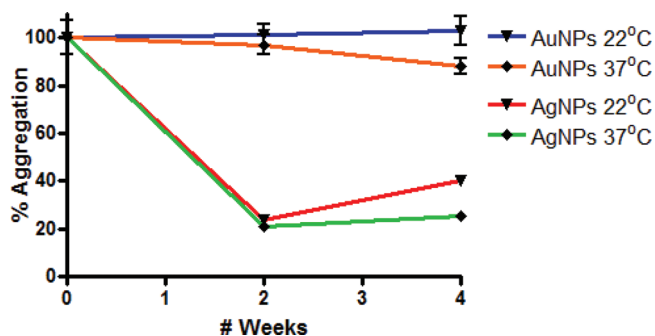


**Figure 6.** Storage stability of Ni(II)NTA NPs. Both the Au and Ag nanoparticles were incubated at variable temperatures in 0.1 M HEPES buffer pH 7.4 with 0.025% Tween 20 for multiple weeks prior to reactions with PLH.

the functionality to coordinate to the Au and Ag surface,<sup>32</sup> while providing a well-ordered packing layer near the NP surface. A poly(ethylene glycol) (PEG) spacer provides a shield between the biological target and NP surface, thus reducing nonspecific interactions between the two.<sup>12</sup> The NTA moiety is attached adjacent to the PEG spacer. To complete the recognition element, Ni(II) is used to charge the chelate to provide the necessary affinity to histidine targets.<sup>22</sup>

A number of factors influence the aggregation behavior of the nanoparticles. These include the affinity of the coordinating ligand to the Ni(II), the  $pK_a$  of the potential coordinating moiety, electrostatics, hydrogen bonding, and the size of the aggregating target molecule. In this study, a systematic investigation of single amino acids, poly(amino acids), and malaria biomarker epitope mimics were used to investigate the aggregation behavior of the Ni(II)NTA Au and AgNPs. A series of acidic and basic monomeric amino acids, including histidine, were incubated with the Ni(II)-charged particles at pH 5.5, 7.4, and 9.0 (Supporting Information). No aggregation behavior was observed for any of the single amino acids across the entire pH range, consistent with the simple coordinative saturation of the Ni(II) binding site. Previous work conducted by Bae et al. showed that 3–5 nm metal-free (uncharged) NTA-NPs did aggregate in the presence of monomeric histidine at pH 9, presumably through hydrogen bonding and electrostatic interactions.<sup>5</sup> When Ni(II) was titrated into their reactions, the aggregation was inhibited. Thus, those single amino acids coordinating to Ni(II) simply saturate the coordination sites on the nanoparticle, resulting in no cross-linked aggregation.

The Ni(II)NTA NPs were then reacted with a variety of commercially available poly(amino acid)s known to have an affinity to Ni(II)NTA. Consistent with the idea that multivalent targets induce the required cross-links for aggregation, each of the basic poly(amino acid) ligands induced aggregation of the nanoparticles at each of the pH's tested, while poly(L-aspartic acid) (PLD) did not. It is likely that the multivalent carboxylic acids outcompete NTA for binding of the Ni(II) ion and subsequently leach it from the nanoparticle, much like EDTA strips Ni(II) from an Ni(II)NTA agarose column.<sup>22</sup> As aggregation could be inhibited above pH 7 by high concentrations of imidazole (data not shown), these poly(amino acid)s likely serve as coordinative cross-links between nanoparticles. In contrast, a different behavior was observed for the protein mimics of malaria.

When the smaller malaria mimics, pHRP-II and BNT-II, were reacted with Ni(II)NTA NPs, the aggregation behavior of the NPs was very sensitive to the pH of the solution. Indeed, BNT-II

and pHRP-II only induced aggregation at pH's below 6, showing a marked decrease in aggregation at pH's higher than the  $pK_a$  of histidine. The large ~8000 MW amino acid PLH polymer induced aggregation of the particles throughout the pH range tested. This difference suggests that the smaller, globular mimics are aggregating through a mechanism different than only simple coordinative cross-linking. At the  $pK_a$  of histidine, 50% of the imidazole rings are deprotonated and available to coordinate the Ni(II) within the functionalized NP's. The other 50% are protonated and available for the formation of hydrogen bonds to deprotonated histidines on other mimic molecules or electrostatic cross-links. The resulting composite is likely an aggregate of mimics coordinated to the Ni(II) of the NPs and cross-linked to other target mimic molecules through hydrogen-bonding and electrostatic interactions. Similar pH-dependent assembly of multivalent histidine-coated nanoparticles has been previously observed.<sup>33</sup> At higher pH, the small peptide mimics simply saturatively coordinate the Ni(II) sites covering the nanoparticles, effectively blocking aggregation. Unlike the larger amino acid polymers, the small size of these mimics prevents particle–particle cross-links due to repulsive particle–particle forces. Consequently, little aggregation is seen above pH 6.

A requirement for the ultimate application of these functionalized nanoparticles in diagnostic assays is that nonspecific interactions between the nanoparticles and other components found in a complex biological matrix do not induce aggregation. Current RDTs for malaria target pfHRP-II in either whole blood or saliva from an infected patient.<sup>1</sup> Within such complex mixtures are proteins (e.g., HRG, TF, HSA, and  $\alpha_2$ ) which are known to have some affinity to M(II)NTA columns at neutral pH.<sup>24</sup> For example, HRG is a 75 kDa protein (507 amino acids) found in relatively high concentrations in human serum (100–200  $\mu\text{g}/\text{mL}$ ).<sup>34</sup> Of the six domains that make up the HRG protein, only the 60 amino acid region of the histidine-rich region (HRR) contains tandem repeats of histidine.<sup>35</sup> Within this region, there are conserved repeats of GHHPH, which serve as  $\text{Zn}^{2+}$  and heme binding domains. Much like pfHRP-II, HRG has been readily purified from serum using Ni(II)NTA agarose affinity chromatography.<sup>36</sup> However, the experimental evidence suggests that neither HRG nor HSA induces aggregation of the particles at pH 5.5, where aggregation was observed for the pfHRP-II mimics. In the case of HRG, the localization of the histidine-rich site concentrated in a single protein domain, as opposed to the complete distribution of such sites in pfHRP-II, limits possible cross-linked driven particle aggregation. Furthermore, at low pH, these control proteins will be protonated, thereby reducing their ability to coordinate with Ni(II)NTA. Similarly, the negative control HSA protein did not induce aggregation of the nanoparticles. In addition, aggregation of the particles with target was readily observed in solutions containing physiological concentrations of HSA, suggesting that HSA has minimal interaction with the particles. Ni(II)NTA Au and AgNPs achieved optimum aggregation upon BNT-II exposure in the presence of varying concentrations of HSA. Aggregation of particles at physiological concentrations of HSA with varying concentrations of BNT-II also revealed that the limit of detection for Au and AgNPs did not significantly change. Finally, both Au and AgNPs underwent aggregation at different particle concentrations, further suggesting HSA does not block target-induced aggregation (Supporting Information).

One of the primary advantages of using metal chelation-based molecular recognition is the avoidance of thermally sensitive reagents such as antibodies. Ni(II)NTA AuNPs stored for a

month suspended in 0.1 M HEPES buffer pH 7.4 with 0.025% Tween 20 either at room temperature or at 37 °C exhibited no change in their spectral profile over time, suggesting that the particles are thermally stable. In addition, their aggregation behavior in the presence of PLH was very similar throughout the thermal time study. In contrast, Ni(II)NTA AgNPs under the same storage conditions appeared to be destabilized after 2 weeks of storage independent of storage conditions. The instability of the Ni(II)NTA AgNPs over extended periods of time can be attributed to several factors. Silver nanoparticles are more susceptible to oxidation at all temperatures in comparison to gold nanoparticles, therefore limiting their shelf life.<sup>37</sup> Further, the self-assembly of alkylthiolates onto silver surfaces is significantly different in comparison to gold. Surface plasmon Raman spectroscopy and *ab initio* calculations demonstrate that alkylthiolates assemble nearly perpendicular to the silver surface, while alkylthiolates assemble  $\sim 30^\circ$  to the normal onto gold surfaces. As a result, monolayers on gold not only take advantage of more efficient packing via van der Waals interactions, but the subsequent S–C bond is less strained.<sup>38</sup> Therefore, only Ni(II)NTA AuNPs demonstrate the potential thermal and storage stability required for further development in global health applications.

## CONCLUSION

Herein, we have highlighted the ease of preparation and use of Ni(II)NTA NPs as a colorimetric diagnostic for histidine-rich proteins. The selectivity and specificity of the Ni(II)NTA construct toward histidine-rich targets were demonstrated over a wide variety of conditions. These particles aggregate in the presence of poly(L-histidine) and malaria biomarker *pf*HRP-II mimics, making them potential colorimetric reagents for malaria RDT's. Furthermore, human serum proteins do not induce aggregation of the particles at low pH, suggesting that the Ni(II)NTA NPs could be further developed to detect *pf*HRP-II in human serum or saliva. A final advantage of the Ni(II)NTA AuNP system is that it demonstrates excellent thermal stability at environmentally relevant conditions over time.

One of the goals of this aggregation reagent is to develop a thermally stable assay component that circumvents the challenges associated with current lateral flow rapid diagnostic tests. Although promising, the proposed reagent currently detects *pf*HRP-II mimics 1 order of magnitude above the World Health Organization's recommended sensitivity of a 2000 parasites/ $\mu$ L parasitemia. These parasite loads correspond to an approximate *pf*HRP-II concentration near 1 nM.<sup>39–42</sup> Even though the current format does not achieve the detection limits needed for a field ready diagnostic, the modularity of the system allows for modifications that will lead to improved sensitivity.

Currently, studies are being performed to investigate the impact of particle size, mixed ligand compositions on the nanoparticle surface, structure of the NTA thiol ligand, and different metal centers (i.e., Co(II), Zn(II), etc.) on the specificity and sensitivity of the system. In addition, sample processing technologies are concurrently being developed to purify and concentrate antigens from complex biological mixtures, such as plasma and whole blood. Together, this processing technology could be coupled with the colorimetric reagent to detect *pf*HRP-II from whole blood in a simple and self-contained diagnostic for use in the developing world.

## EXPERIMENTAL SECTION

**Reagents.** Au and AgNPs were purchased from Ted Pella Inc. All peptide reagents were purchased from Aapptec Inc. Antibodies for HRG characterization were purchased from Abcam Inc. Western blotting reagents were purchased from Invitrogen Inc. All other reagents were purchased from Fisher Scientific Inc. or Sigma-Aldrich Inc. and used without modification.

**Synthesis of Ni(II)NTA Silver Nanoparticles (AgNPs).** A 115  $\mu$ M solution of citrate-capped silver nanoparticles was incubated with 10  $\mu$ M of 7 overnight at room temperature. The particles were then centrifuged (20 min, 5000g) and washed three times with 0.1 M HEPES buffer with 0.25% Tween-20 (pH 7.4). Next, the silver nanoparticles were incubated in a 10  $\mu$ M NiCl<sub>2</sub>·6H<sub>2</sub>O solution overnight at room temperature to coordinate Ni(II) to 7. The particles underwent three additional centrifuge purification cycles (20 min, 5000g), in which they were resuspended in 0.1 M HEPES with 0.025% Tween-20. For the pH studies, the particles were resuspended in 0.1 M MES buffer (pH 5.5) with 0.025% Tween-20 or 0.1 M CHES buffer (pH 9.0) with 0.025% Tween-20. The final particle concentration for all studies was adjusted to  $\sim 100$  pM, as confirmed by UV–vis spectrophotometry.

**Synthesis of NiNTA AuNPs.** A 2.3 nM solution of citrate-stabilized AuNPs (15 nm) was incubated with 0.2 mM NTA-thiol ligand overnight at room temperature. After the initial loading period, the resulting solution was centrifuged (45 min, 7200g) to remove the unreacted thiols and washed three times with 0.1 M HEPES buffer (pH 7.4) with 0.25% Tween-20. The resuspended particles were charged with Ni(II) upon the addition of 0.2 mM NiCl<sub>2</sub> and incubated overnight. Next, the particles were centrifuged and washed three additional times with the final suspension buffer (0.1 M HEPES, 0.025% Tween 20) before storage or use. For the pH studies, the final suspension buffer for pH 5.5 was 0.1 M MES buffer, 0.025% Tween 20 and for pH 9.0 was 0.1 M CHES buffer, 0.025% Tween 20.

**Characterization of Ni(II)NTA NPs.** All particles synthesized in this study were characterized by TEM using a Phillips CM20 microscope. Size distribution of the particles were determined by dynamic laser scattering (DLS) using a Malvern Nano ZS. Spectral characterization was performed on either an Agilent 8453 UV–vis spectrometer or a Bio-Tek Synergy HT plate reader.

**Synthesis of Protein Mimics.** All peptides were synthesized using standard Fmoc solid phase synthesis methods using an Apex 396 peptide synthesizer (Aapptec). BNT-II was synthesized using previously established methods using a MAP resin containing four branches.<sup>31</sup> All linear peptides were synthesized using a Rink amide resin. The N-terminus of each peptide was acylated using DCM:acetic anhydride (1:1). Cleavage was performed by treating the functionalized resins with Reagent R (90:5:3:2 TFA:thioanisole:anisole:EDT) and precipitating the peptides in cold ether. Purification was performed using a reverse-phase HPLC (Waters Prep LC 4000) with a Waters 2487 dual wavelength detector and C18 column. The purified products were characterized using MALDI-TOF and tested for activity against a rapid diagnostic test specific for *pf*HRP-II (Malaria Antigen *Pf*, Standard Diagnostics, Inc.).

**Purification of Histidine-Rich Glycoprotein (HRG).** Human HRG was purified from plasma (Valley Biomedical) by Ni(II)NTA (Qiagen) affinity chromatography. Plasma (45 mL) was loaded onto a pre-equilibrated column of Ni(II)NTA resin (5 mL) and incubated at 4 °C overnight with shaking. This reaction mixture contained 50 mM imidazole during incubation. After incubation, the resin was washed with 10 column volumes of 50 mM phosphate buffer, pH 8.0, with 500 mM NaCl and 50 mM imidazole. Next, the proteins were eluted using a gradient of imidazole up to 500 mM. After pooling fractions containing HRG, they were concentrated using Amicon centrifuge filtration units (30 kDa MW cutoff) and washed with 0.1 M HEPES, pH 7.4. The concentration of the protein was determined using the Bradford assay.

Confirmation of the product was determined by SDS-PAGE using a 4–10% Bis-Tris gel.

**Western Blot of HRG.** Western blotting was also performed by running HRG on SDS-PAGE and subsequently transferring to a PVDF membrane (Invitrogen). The membrane was then blocked with 5% skimmed milk in 10 mM Tris, 0.15 M NaCl, pH 7.4, 0.1% Tween 20 (TBST) overnight at 4 °C. Next, a 1:1000 dilution of HRG rabbit primary antibody (Abcam) was added and incubated for 1 h at room temperature. After washing 5 times with TBST, the membrane was incubated with 0.5  $\mu$ g/mL HRP conjugated secondary anti-rabbit IgG antibody for 1 h. After subsequent washes with TBST, the image was developed using the ECL system (Invitrogen).

**Titration Assays.** Aggregation behavior of Ni(II)NTA NPs was performed by titrating various amounts of targets with the particles. Briefly, targets were added to the NPs (Au, 2.75 nM; Ag, 0.1 nM) and incubated for 15 min while being monitored by UV–vis and/or DLS. Note: preliminary studies were performed using a checkerboard assay to determine the optimal nanoparticle concentration for this study.

**Synthesis of NTA-Thiol Ligand.** Synthesis of the NTA-thiol ligand **7** is summarized in Scheme 2. It follows procedures developed by Schmitt et al.<sup>28</sup> and Tinazli et al.<sup>29</sup> Briefly, 11-mercaptoundecanoic acid (**1**) was protected by treatment with zinc acetate to yield 11-acetylsulfanylundecanoic acid (**2**). Next, **2** was coupled to triethylene glycol using DCC coupling chemistry in DCM to afford **3**. The terminal alcohol of **3** was then activated with carbonyldiimidazole (CDI) in DCM to generate the imidazolid intermediate **5**. After purification, **5** was nucleophilically attacked with the NTA lysine moiety **4** synthesized using the method developed by Schmitt et al.<sup>43</sup> to yield the protected NTA product **6**. Final deprotection of the NTA-thiol ligand **7** was achieved with hydrazine acetate in DMF. Total yield under these conditions was 44.7%.

**S-Acetyl-MUA (2).** 11-Mercaptoundecanoic acid (MUA) (5.00 g, 21.75 mmol, Sigma, 95%) (**1**) was dissolved in DCM (60 mL) and AcOH (60 mL). Subsequently, Zn (10 g) was added to the reaction mixture and incubated for 15 min. The reaction mixture was then cooled to 0 °C prior to the addition of 30 mL of acetyl chloride (425 mmol). After 2 h of incubation, the reaction mixture was warmed to room temperature, and the reaction solution was separated from the Zn by filtration. Next, the organic solution was washed twice with chilled 0.1 M HCl, and the solvent was evaporated. The crude product was purified by silica chromatography. TLC:  $R_f$  = 0.54 (ethyl acetate). Yield 5.25 g (88%). <sup>1</sup>H NMR (CDCl<sub>3</sub>):  $\delta$ : 2.83 (t, 2H), 2.32 (t, 2H), 2.30 (s, 3H), 1.5–1.62 (m, 4H), 1.2–1.4 (m, 12H).

**S-Acetyl-MUA-PEG-OH (3).** To a solution of **2** in DCM (5.25 g, 20.2 mmol), triethylene glycol (27.5 mL, 20.6 mmol) and DMAP (0.52 g, 4.26 mmol) were added, followed by the addition of DCC (5.51 g, 26.7 mmol). The reaction mixture was stirred overnight. The reaction mixture was then filtered to remove any urea, and the organic solution was washed with 0.1 M HCl. The aqueous layer was extracted once with DCM. The combined organic phases were dried over Na<sub>2</sub>SO<sub>4</sub>, and the solvent was evaporated. The crude product **3** was purified by chromatography using ethyl acetate as the eluent. TLC:  $R_f$  = 0.49 (ethyl acetate). Yield 5.7 g (72%). <sup>1</sup>H NMR (CDCl<sub>3</sub>):  $\delta$ : 4.22 (t, 2H), 3.6–3.75 (m, 10H), 2.86 (t, 2H), 2.32 (t, 2H), 2.31 (s, 3H), 1.5–1.62 (m, 4H), 1.2–1.4 (m, 12H).

**S-Acetyl-MUA-PEG-imidazolide (4).** To a 20 mL solution of **3** in DCM (2.85 g, 7.27 mmol), 2.35 g of carbonyldiimidazolide (CDI, 14.5 mmol) was added and incubated for 4 h. The imidazolide product **4** was then purified by silica column chromatography using first a gradient of 50:50 hexane:ethyl acetate followed by ethyl acetate. Yield 3.00 g (84.7%). TLC:  $R_f$  = 0.57 (ethyl acetate). <sup>1</sup>H NMR (CDCl<sub>3</sub>):  $\delta$ : 8.30 (s, 1H), 7.60 (d, 1H), 7.06 (d, 1H), 4.57 (t, 2H), 4.17 (t, 2H), 3.85 (t, 2H), 3.6–3.7 (m, 6H), 2.84 (t, 2H), 2.30 (t, 2H), 2.29 (s, 3H), 1.5–1.62 (m, 4H), 1.2–1.4 (m, 12H). MS: 487 (ESI<sup>+</sup>) (MH<sup>+</sup>).

**S-Acetyl-MUA-PEG-NTA (6).** Na,N<sub>2</sub>-Methylcarboxy-L-lysine (1.4 g, 5.34 mmol), synthesized according the method of Schmitt et al.,<sup>43</sup> was dissolved in 15 mL of water, and the pH was adjusted to 10 with concentrated NaOH. This solution was mixed with 650 mg (1.33 mmol) of **4** in 15 mL of DMF and incubated overnight. The reaction was quenched with 15 mL of water, and the aqueous solution was extracted three times with ethyl acetate. The aqueous phase was then acidified to pH 1.5 with 0.1 M HCl and extracted four times with ethyl acetate. The combined organic fractions were washed with saturated sodium chloride and dried over anhydrous Na<sub>2</sub>SO<sub>4</sub>. Finally, the organic solvent was removed by vacuum. Yield 970 mg (quant). <sup>1</sup>H NMR (MeOD)  $\delta$ : 4.19 (t, 2H), 4.15 (t, 2H), 3.5–3.8 (m, 13H), 3.11 (t, 2H), 3.07 (m, 2H), 2.85 (t, 2H), 2.32 (t, 2H), 2.29 (s, 3H), 1.5–1.62 (m, 8H), 1.2–1.4 (m, 14H). MS: 681 (ESI<sup>+</sup>) (MH<sup>+</sup>Na<sup>+</sup>), 703 (ESI<sup>+</sup>) (MH<sup>+</sup>2Na<sup>+</sup>).

**MUA-PEG-NTA (7).** Hydrazine acetate (140 mg, 1.5 mmol) was added to a 100 mg (0.15 mmol) solution of **6** in DMF under nitrogen. The reaction mixture was mixed overnight, and the solvent was evaporated. The crude product **7** was resuspended in water and acidified until a precipitate formed (pH = 1.5). The precipitated product was then extracted three times using ethyl acetate. The combined organic fractions were dried using anhydrous sodium sulfate, and the solvent was evaporated. The final product was then resuspended in water and lyophilized overnight. Yield 79.6 mg (83.2%). <sup>1</sup>H NMR (D<sub>2</sub>O)  $\delta$ : 4.19 (t, 2H), 4.13 (t, 2H), 3.5–3.8 (m, 13H), 3.11 (t, 2H), 3.06 (m, 2H), 2.67 (t, 1H), 2.48 (t, 2H), 2.32 (t, 2H), 1.5–1.65 (m, 8H), 1.2–1.4 (m, 14H). MS: 637 (ESI<sup>-</sup>) (M<sup>-</sup>), 639 (ESI<sup>+</sup>) (MH<sup>+</sup>), 661 (ESI<sup>+</sup>) (MH<sup>+</sup>Na<sup>+</sup>).

## ■ ASSOCIATED CONTENT

Supporting Information. Additional figures as described in the text. This material is available free of charge via the Internet at <http://pubs.acs.org>.

## ■ AUTHOR INFORMATION

### Corresponding Author

\*Fax 615-343-1234; Tel 615-322-2636; e-mail David.Wright@Vanderbilt.edu.

## ■ ACKNOWLEDGMENT

Support for this research was provided by the Bill and Melinda Gates Foundation Grand Challenges Exploration grant and Vanderbilt University. The authors thank M. F. Richards for critical comments concerning the manuscript.

## ■ REFERENCES

- (1) Moody, A. *Clin. Microbiol. Rev.* **2002**, *15*, 66.
- (2) WHO, *Malaria Rapid Diagnostic Test Performance*, 2008.
- (3) Elghanian, R.; Storhoff, J. J.; Mucic, R. C.; Letsinger, R. L.; Mirkin, C. A. *Science* **1997**, *277*, 1078.
- (4) Gao, J.; Fu, J.; Lin, C.; Lin, J.; Han, Y.; Yu, X.; Pan, C. *Langmuir* **2004**, *20*, 9775.
- (5) Bae, D. R.; Han, W. S.; Lim, J. M.; Kang, S.; Lee, J. Y.; Kang, D.; Jung, J. H. *Langmuir* **2009**, *26*, 2181.
- (6) Yu, J. S.; Liao, H. X.; Gerdon, A. E.; Huffman, B.; Scarce, R. M.; McAdams, M.; Alam, S. M.; Popernack, P. M.; Sullivan, N. J.; Wright, D.; Cliffl, D. E.; Nabel, G. J.; Haynes, B. F. *J. Virol. Methods* **2006**, *137*, 219.
- (7) Hainfeld, J. F.; Liu, W. Q.; Halsey, C. M. R.; Freimuth, P.; Powell, R. D. *J. Struct. Biol.* **1999**, *127*, 185.
- (8) Storhoff, J. J.; Elghanian, R.; Mucic, R. C.; Mirkin, C. A.; Letsinger, R. L. *J. Am. Chem. Soc.* **1998**, *120*, 1959.
- (9) Kreibig, U.; Genzel, L. *Surf. Sci.* **1985**, *156*, 678.
- (10) Quinten, M.; Kreibig, U. *Surf. Sci.* **1986**, *172*, 557.

- (11) Prodan, E.; Nordlander, P. *J. Chem. Phys.* **2004**, *120*, 5444.
- (12) Wuelfing, W. P.; Gross, S. M.; Miles, D. T.; Murray, R. W. *J. Am. Chem. Soc.* **1998**, *120*, 12696.
- (13) Cho, K.; Lee, Y.; Lee, C. H.; Lee, K.; Kim, Y.; Choi, H.; Ryu, P. D.; Lee, S. Y.; Joo, S. W. *J. Phys. Chem. C* **2008**, *112*, 8629.
- (14) Liu, D. B.; Qu, W. S.; Chen, W. W.; Zhang, W.; Wang, Z.; Jiang, X. Y. *Anal. Chem.* **2010**, *82*, 9606.
- (15) Hung, Y. L.; Hsiung, T. M.; Chen, Y. Y.; Huang, Y. F.; Huang, C. C. *J. Phys. Chem. C* **2010**, *114*, 16329.
- (16) Kalluri, J. R.; Arbneshi, T.; Khan, S. A.; Neely, A.; Candice, P.; Varisli, B.; Washington, M.; McAfee, S.; Robinson, B.; Banerjee, S.; Singh, A. K.; Senapati, D.; Ray, P. C. *Angew. Chem., Int. Ed.* **2009**, *48*, 9668.
- (17) Tsai, C. S.; Yu, T. B.; Chen, C. T. *Chem. Commun. (Cambridge, U. K.)* **2005**, 4273.
- (18) Zhang, X.; Kong, X.; Fan, W.; Du, X. *Langmuir* **2011**, *27*, 6504.
- (19) Terpe, K. *Appl. Microbiol. Biotechnol.* **2003**, *60*, 523.
- (20) Mori, S.; Takahashi, H. K.; Yamaoka, K.; Okamoto, M.; Nishibori, M. *Life Sci.* **2003**, *73*, 93.
- (21) Ghimire, P.; Samantaray, J. C.; Mirdha, B. R.; Patra, A. K.; Panda, A. K. *Southeast Asian J. Trop. Med. Public Health* **2003**, *34*, 739.
- (22) Knecht, S.; Ricklin, D.; Eberle, A. N.; Ernst, B. *J. Mol. Recognit.* **2009**, *22*, 270.
- (23) De, M.; Rana, S.; Rotello, V. M. *Macromol. Biosci.* **2009**, *9*, 174.
- (24) Pantou, L. J.; McPhie, P.; Maloy, W. L.; Wellem, T. E.; Taylor, D. W.; Howard, R. J. *Mol. Biochem. Parasitol.* **1989**, *35*, 149.
- (25) Chiodini, P. L.; Bowers, K.; Jorgensen, P.; Barnwell, J. W.; Grady, K. K.; Luchavez, J.; Moody, A. H.; Cenizal, A.; Bell, D. *Trans. R. Soc. Trop. Med. Hyg.* **2007**, *101*, 331.
- (26) Schneider, E. L.; Marletta, M. A. *Biochemistry* **2005**, *44*, 979.
- (27) Barton, C. S.; Waniganayake, L.; Wie, G.; McMurchie, E. J.; Leifert, W. R.; Jamting, A.; Raguse, B.; Weiczorek, L. *ICONN* **2006**.
- (28) Schmitt, L.; Ludwig, M.; Gaub, H. E.; Tampe, R. *Biophys. J.* **2000**, *78*, 3275.
- (29) Tinazli, A.; Tang, J. L.; Valiokas, R.; Picuric, S.; Lata, S.; Piehler, J.; Liedberg, B.; Tampe, R. *Chem.—Eur. J.* **2005**, *11*, 5249.
- (30) Mulvaney, P. *Langmuir* **1996**, *12*, 788.
- (31) Ziegler, J.; Chang, R. T.; Wright, D. W. *J. Am. Chem. Soc.* **1999**, *121*, 2395.
- (32) Nuzzo, R. G.; Zegarski, B. R.; Dubois, L. H. *J. Am. Chem. Soc.* **1987**, *109*, 733.
- (33) Slocik, J. M. PhD Thesis (in Chemistry), Vanderbilt University, Dec 2004.
- (34) Heimburger, N.; Haupt, H.; Kranz, T.; Baudner, S. *Hoppe Seylers Z. Physiol. Chem.* **1972**, *353*, 1133.
- (35) Jones, A. L.; Hulett, M. D.; Parish, C. R. *Immunol. Cell Biol.* **2005**, *83*, 106.
- (36) Manderson, G. A.; Martin, M.; Onnerfjord, P.; Saxne, T.; Schmidtchen, A.; Mollnes, T. E.; Heinegard, D.; Blom, A. M. *Mol. Immunol.* **2009**, *46*, 3388.
- (37) Aslan, K.; Malyn, S. N.; Geddes, C. D. *J. Fluoresc.* **2007**, *17*, 7.
- (38) Sellers, H.; Ulman, A.; Shnidman, Y.; Eilers, J. E. *J. Am. Chem. Soc.* **1993**, *115*, 9389.
- (39) Minigo, G.; Woodberry, T.; Piera, K. A.; Salwati, E.; Tjitra, E.; Kenangalem, E.; Price, R. N.; Engwerda, C. R.; Anstey, N. M.; Plebanski, M. *PLoS Pathog.* **2009**, *5*, e1000402.
- (40) Dondorp, A. M.; Desakorn, V.; Pongtavornpinyo, W.; Sahassananda, D.; Silamut, K.; Chotivanich, K.; Newton, P. N.; Pitisuttithum, P.; Smithyman, A. M.; White, N. J.; Day, N. P. *PLoS Med.* **2005**, *2*, e204.
- (41) Martin, S. K.; Rajasekariah, G. H.; Awinda, G.; Waitumbi, J.; Kifude, C. *Am. J. Trop. Med. Hyg.* **2009**, *80*, 516.
- (42) Kifude, C. M.; Rajasekariah, H. G.; Sullivan, D. J., Jr.; Stewart, V. A.; Angov, E.; Martin, S. K.; Diggs, C. L.; Waitumbi, J. N. *Clin. Vaccine Immunol.* **2008**, *15*, 1012.
- (43) Schmitt, L.; Dietrich, C.; Tampe, R. *J. Am. Chem. Soc.* **1994**, *116*, 8485.